HHS Public Access

Author manuscript

Arterioscler Thromb Vasc Biol. Author manuscript; available in PMC 2020 October 01.

Published in final edited form as:

Arterioscler Thromb Vasc Biol. 2019 October ; 39(10): 2067–2081. doi:10.1161/ATVBAHA.119.313077.

Adamts5$^{-/-}$ Mice Exhibit Altered Aggrecan Proteolytic Profiles That Correlate with Ascending Aortic Anomalies

Loren E. Dupuis[1], **E. Lockett Nelson**[1], **Brittany Hozik**[1], **Sarah C. Porto**[1], **Alexandra Rogers-DeCotes**[1], **Amanda Fosang**[2], **Christine B. Kern**[1,*]

[1]Department of Regenerative Medicine and Cell Biology, Medical University of South Carolina, Charleston, SC 29464, Australia

[2]Department of Paediatrics, University of Melbourne, the Murdoch Children's Research Institute, Royal Children's Hospital, Parkville 3052, Australia

Abstract

Objective—Investigate the requirement of aggrecan cleavage during aortic wall development in a murine model with ADAMTS5 deficiency and bicuspid aortic valves.

Approach—Mice with altered extracellular matrix remodeling of proteoglycans will be examined for anomalies in ascending aortic wall development. Neo-epitope antibodies that recognize ADAMTS cleaved Acan fragments will be used to investigate the mechanistic requirement of Acan turnover, in aortic wall development.

Results—*Adamts5*$^{-/-}$*;Smad2*$^{+/-}$ mice exhibited a high penetrance of aortic anomalies (n=17/17); *Adamts5*$^{-/-}$*;Smad2*$^{+/-}$ mice with bicuspid aortic valves (7/17) showed a higher number of anomalies than *Adamts5*$^{-/-}$*;Smad2*$^{+/-}$ mice with tricuspid aortic valves. Single mutant *Adamts5*$^{-/-}$ mice also displayed a high penetrance of aortic anomalies (n=19/19) compared with wild type (WT) (n=1/11). Aortic anomalies correlated with Acan accumulation that was apparent at the onset of elastogenesis in *Adamts5*$^{-/-}$ mice. Neo-epitope antibodies that recognize the initial Acan cleaved fragments neo-FREEE, neo-GLGS and neo-SSELE, were increased in the *Adamts5*$^{-/-}$aortas compared with wild type. Conversely, neo-TEGE, that recognizes highly digested Acan core fragments, was reduced in *Adamts5*$^{-/-}$ mice. However, mice containing a mutation in the TEGE$_{373}\downarrow_{374}$ALGSV site, rendering it non-cleavable, had low penetrance of aortic anomalies (n=2/4). Acan neo-DIPEN and neo-FFGVG fragments were observed in the aortic adventitia; Acan neo-FFGVG was increased abnormally in the medial layer and overlapped with smooth muscle cell loss in *Adamts5*$^{-/-}$ aortas.

Conclusions—Disruption of ADAMTS5 Acan cleavage during development correlates with ascending aortic anomalies. These data indicate that the mechanism of ADAMTS5 Acan cleavage may be critical for normal aortic wall development.

Cover Art

*Corresponding Author 171 Ashley Avenue BSB647, Charleston, SC 29425, kernc@musc.edu, 843 792-9618.

Disclosures: none.

The image shows the ascending aorta of mice deficient in the extracellular matrix protease ADAMTS5. Aggrecan, (green) a large aggregating proteoglycan accumulates during development of the ascending aorta on the adventitial side of the smooth muscle cells (blue) and correlates with ascending aortic anomalies. Nuclei are stained with propidium iodide (red).

Graphical Abstract

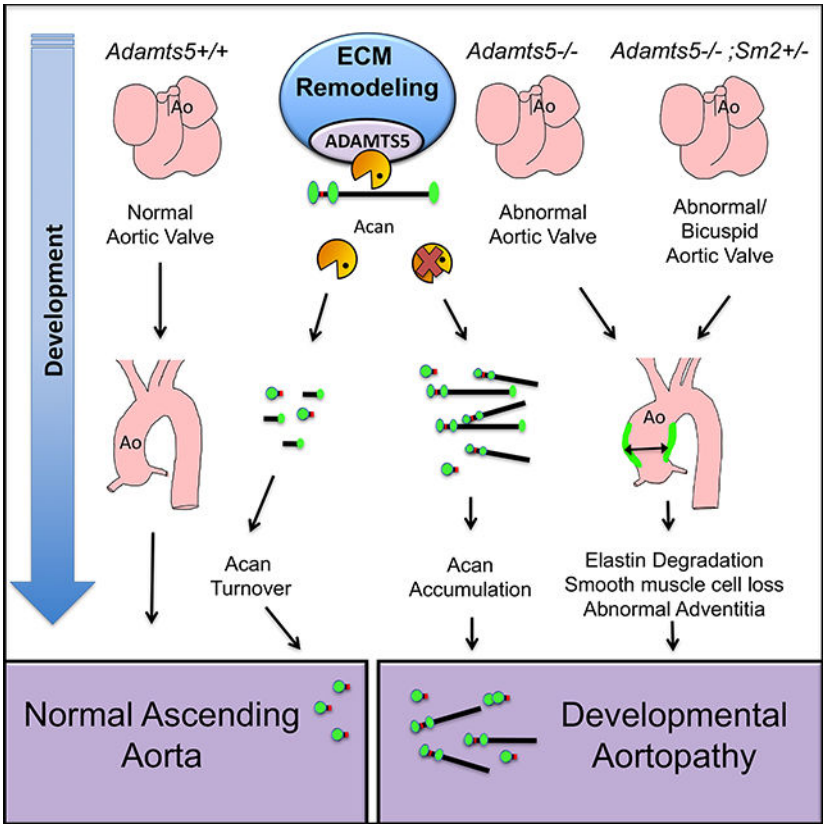

Keywords

Aorta; Aggrecan; ADAMTS5; Bicuspid; neo-epitope

Subject codes

developmental biology; vascular biology; genetically altered and transgenic models; aortic dissection

Introduction

The dissection and rupture of thoracic aortic aneurysms has an incidence of approximately 7 in 100,000 people per year [1] and are often asymptomatic, contributing to the high rate of morbidity and mortality. Patients with a bicuspid aortic valve (BAV) rather than the normal tricuspid have a higher incidence of aortopathies that lead to sudden death [2]. However, the progression of thoracic aortic aneurysms is heterogeneous, making it difficult to predict the

need for surgical intervention. Understanding mechanisms involved in normal aortic wall development may elucidate biomarkers for prediction of disease progression and identify novel therapeutic targets for the treatment of ascending aortic aneurysms.

Histological examination of aneurysmal aortas demonstrates vascular smooth muscle cell (SMC) apoptosis and disorganization of the ECM. There is a significant body of evidence that links ECM remodeling with vascular diseases [3, 4]. Aortic aneurysms can display high levels of matrix metalloproteases (MMPs), which degrade elastin in both animal models and in patient samples of end stage disease. [5–7]. In addition to the MMPs, the ADAMTS-1, 4, 5 proteases have been implicated in thoracic aortic aneurysms [8–10]. ADAMTS-1, −4, and −5 are the main enzymes responsible for cleavage of the large aggregating proteoglycans, aggrecan (Acan) and versican (Vcan) [11]. ADAMTS5 is reduced in a murine model of atherosclerosis, in part through regulation of biglycan and versican levels in *apoE*$^{-/-}$ mice [12]. Massive accumulation of Acan, is also present in ruptured aortic tissue of thoracic aortic aneurysm patients, but not in healthy aortic tissue [10]. Acan is generally associated with cartilage, where it complexes with hyaluronan (HA) and link protein to form gigantic ECM complexes that contribute to its rigid structure. In fact, therapeutics for the reduction of ADAMTS5-mediated Acan cleavage in joints, has reached clinical trials to treat osteoarthritis [13].

Investigation using ECM protease deficient mice can provide *in vivo* validation for ECM substrates essential in the arterial wall, that have been characterized largely *in vitro*. A proteomics approach that compares the ECM of aortas from mice lacking the catalytic domain of ADAMTS5, to aortas from littermate controls revealed an accumulation of Acan. The structural changes in the aortic wall were accompanied by an increase in the diameter of the thoracic but not the abdominal aorta [14]. When hypertension is induced in *Adamts5*$^{-/-}$ mice with Ang II, aortic dilation was increased in *Adamts5*$^{-/-}$ mice in the aortic root, annulus and the ascending aorta compared to wild type (WT) [15]. Previous work from our laboratory demonstrates that loss of ADAMTS5 results in cardiac valve defects due to accumulation of its proteoglycan substrate Vcan [16]. However, an intergenetic cross of *Adamts5*$^{-/-}$ mice with *Vcan*$^{+/-}$, which produces less Vcan, rescues the *Adamts5*$^{-/-}$ cardiac valve phenotype indicating that accumulation of its substrate Vcan is a primary factor in the valve malformations. Cardiac valves from developing *Adamts5*$^{-/-}$ mice contain prevalvular mesenchymal cells that exhibit a reduction of pSmad2 and its downstream ECM targets including Collagen I [16]. When Smad2 was reduced through an intergenetic cross with *Adamts5*$^{-/-}$ mice, the *Adamts5*$^{-/-}$*;Smad2*$^{+/-}$ mice develop more severe pulmonary and aortic valve malformations than the single *Adamts5*$^{-/-}$ mutant mice with highly penetrant bicuspid aortic valve (75%) and bicuspid pulmonary valve (65%) [17]. In this study, we investigate the hypothesis that ADAMTS5 mediated cleavage of its proteoglycan substrate Acan is required for the normal development of the ascending aorta. Understanding the etiology of ascending aortic anomalies, may lead to effective therapeutic approaches and diagnostic tools for thoracic aortic aneurysms.

Materials and Methods

The data that support the findings of this study are available from the corresponding author upon reasonable request.

Gene-targeted mice

All mouse experiments were done under protocols approved by the Medical University of South Carolina IACUC. The standard twelve-hour light cycle was diurnal and was set for six o'clock am on then 6 o'clock pm off. There was unlimited access to food and water, supplied via reverse osmosis system and dispensed into Lab Product rodent bottles/sippers. Purina Lab Diet 5V75 (standard diet) and 5VM5 (breeder diet) was utilized with unlimited supply and access. The bedding source is autoclaved corn cob (Bed'o'Cobs) supplied by Anderson Lab Bedding. The *Adamts5*$^{-/-}$ mice used in this study were the *Adamts5*$^{tm1Dgen/J}$ (The Jackson Laboratory, Bar Harbor, ME) that were bred into C57BL/6J (> 10 generations) and maintained as previously described [18, 19]. Genotyping of *Adamts5* mice was performed using PCR as previously published [19]. *Smad2*$^{+/-}$ mice were also maintained on a pure C57BL/6J background. Developmental tissue evaluated in this study was obtained from *Adamts5*$^{+/-}$/*Smad2*$^{+/-}$ X *Adamts5*$^{+/-}$/*Smad2*$^{+/+}$ intercross matings. Six-month-old male and female mice were used in the adult study, as indicated in Figure 2. Hearts from mice containing a knock-in mutation NVTEGE$_{373}$↓$_{374}$ALGSV site that rendered this site non-cleavable [20] were obtained from Dr. Fosang, these mice were maintained under protocols approved by the University of Melbourne IACUC and are on a C57BL/6J background.

Scoring of aortic anomalies

All hearts with the ascending aortic and pulmonary arteries attached anterior to the aortic arch, were removed from the body cavity, fixed in 4% paraformaldehyde or alcohol/acetic acid/methanol, and embedded in the frontal plane with the ventral side in anatomical position down in the paraffin block. Stenosis was scored by examining the aortic diameter at the opening to the left ventricle. If there was a narrowing of the width of the aortic opening to the left ventricle that was significantly smaller than the average of the wild type, it was denoted as stenotic. An anomaly in outflow tract rotation was indicated by an altered placement i.e. malpositioning over the interventricular septum rather than the left ventricular lumen. Membranous interventricular septal defect was indicated by altered geometry or a thin membranous flap, where the normal muscularized wall is formed in wild type mice. Bicuspid phenotypic scoring of murine aortic and pulmonary valves: The phenotype from *Adamts5*$^{+/-}$/*Smad2*$^{+/-}$ X *Adamts5*$^{+/-}$/*Smad2*$^{+/+}$ crosses was scored as bicuspid when only two cusps were noted after examination of all serial sections and/or when there were only two arterial wall-anchoring sites (or commissures) found in the valve. Smooth muscle cell loss and cell infiltration were denoted by obvious alterations in the ascending aortic wall compared to wild type, examples shown in Fig. 1E, 1H, 1K. Dissected aorta was identified by a mass of blood attached to the ascending aorta was observed when the body cavity was opened and the thymus glands removed during dissection, and/or tissue sections of the ascending aortic wall that contained irregularities in the aortic wall along with blood within the adventitial layer, examples given in Fig. 1G, 1I, 1J, 1K, anomalies not present in wild type hearts. Thick aortic wall was denoted as increased thickness compared to the average of

wild type hearts. Statistics and measurement areas shown in Fig. 2. Alterations in aortic geometry were not observed in the frontal plane of any wild type hearts, examples from different *Adamts5*$^{-/-}$ hearts are shown in Fig. 1B, Fig. 3B, and 3C.

Histology and Immunohistochemistry

Standard histological procedures were used [21]. Immunohistological localization utilized the following antibodies: tropoelastin (Abcam, AB21601), Acan [22], GAGβ [21], α-sarcomeric actin (Sigma, A2172), α-smooth muscle actin (Sigma, A5228), myosin light chain kinase (Abcam, ab76092); Acan neo-epitope antibodies neo-FREEE, neo-GLGS, neo-SSELE, neo-TEGE, provided by Dr. Fosang [23, 24] and neo-DIPEN (mdbioproducts 1042002). Histological staining utilized isolated hearts that were fixed in 4% paraformaldehyde or Amsterdam fixative (35% methanol/35% acetone/5% acetic acid) [16]. Flourophore conjugated secondary antibodies were purchased from Jackson ImmunoResearch. For immunohistochemistry, commercially available antibodies have been affinity purified or tested in their respective deletion mutant animal tissue (Please provide references if available). For the Acan core protein the IgG concentration was used as the same antibody concentration in combination with secondary antibodies, and previously published (22). The cleaved Aggrecan neo-epitope antibodies have been characterized previously in Western blots of chondrocytes and affinity purified (23).

Quantification of immunohistochemistry data—To quantify expression from IHC data, digital images of *Adamts5*$^{-/-}$ and wild type heart sections were acquired at identical confocal settings using the Leica TCS SP5 AOBS Confocal Microscope System (Leica Microsystems Inc., Exton, PA). Tissue from WT and *Adamts5*$^{-/-}$ littermates, were processed for embedding coordinately. Subsequent immunohistochemistry was performed in the same experiment, each heart qualifies as n=1, per genotype. A minimum of three separate experiments with four different litters of matched *Adamts5*$^{-/-}$ and WT hearts was used for immunohistochemistry quantification and representative images of immunohistochemistry ECM localization are shown.

Western blots and quantification

Heart extracts from WT and *Adamts5*$^{-/-}$ mice were prepared using standard RIPA buffer extraction plus protease inhibitors. For Acan western blots, 3–8% reducing gradient gels were used. Blots were probed with Acan antibody or neo-epitope antibodies [22]. RIPA lysates were generated from combined developmental dissected ascending aortas, protein was quantified using BCA assay. Equal amounts of lysate (based on protein quantification using the BCA assay) were treated with Chondroitinase ABC, prior to loading on gradient gels. The Western blots shown are representative of n=4 different hearts of each genotype and each developmental stage. In the case of postnatal day 7, two aortas of the same genotype were pooled, counted as n=1 and used in Westerns. In addition, three technical replicates for quantification were performed for each antibody and Western shown.

Statistical Analysis

Graph data are expressed as mean values with error bars depicting the standard deviation of the mean. Differences between the groups of immunohistochemistry positive pixels of Acan

immunofluorescence for adult and P7 was evaluated using student t-test, parametric. If there were significant differences of variances between groups, the Mann-Whitney non-parametric test was used, as in the case of the immunohistochemistry of Acan confocal quantification for adult and P7. The combined male female aortic wall thickness and separate male, female values of aortic wall thickness, that included genotypes *Adamts5*$^{+/+}$;*Smad2*$^{+/-+}$, *Adamts5*$^{-/-}$;*Smad2*$^{+/+}$ *Adamts5*$^{-/-}$;*Smad2*$^{+/-}$ and *Adamts5*$^{+/+}$;*Smad2*$^{+/-}$ were evaluated by one-way ANOVA. Data passed normality and equal variance tests (Brown-Forsythe) using GraphPad Prism 6 (GraphPad Prism Software Inc). Tukey post-hoc tests were performed to identify groups with significant differences. Western quantification was performed by analyzing band density with Image J 1.52k (National Institutes of Health). Data on Acan band densities were normalized using loading controls of each lane. The resulting data was evaluated for statistical significance and graphed using GraphPad Prism. In graphs, significant values are denoted as: *P<0.05; **P<0.01; ***P<0.001, **** P<0.0001.

Results

Ascending aortic anomalies were observed in ADAMTS5 deficient mice

Since bicuspid aortic valves are an independent risk factor for ascending aortic aneurysms, the *Adamts5*$^{-/-}$;*Smad2*$^{+/-}$ (n=17) that have a 75% penetrance bicuspid AV as well as the *Adamts5*$^{-/-}$ (n=19) mice, that have a 12% penetrant bicuspid AV and a fully penetrant myxomatous valve phenotype [17], were examined for ascending aortic artery malformations (Fig. 1). Previously published studies evaluated the ascending aorta using echocardiographic analysis that revealed an increase in thoracic aortic diameter in *Adamts5*$^{-/-}$ mice (14). Upon angiotensin II treatment there was a significant increase in the diameter of the aortic annulus in *Adamts5*$^{-/-}$ mice compared to wild type [14, 15].

Here, analysis of whole hearts of wild type, *Adamts5*$^{-/-}$;*Smad2*$^{+/-}$ and *Adamts5*$^{-/-}$ mice by light microscopy was inconclusive in detecting ascending aortic anomalies (**Supplemental Figure I**). However, there was blood surrounding the ascending aorta in *Adamts5*$^{-/-}$ mice (**Supplemental Figure IG, H**). There was also evidence of a slight lack of rotation of the aorta in *Adamts5*$^{-/-}$ hearts (**Supplemental Figure ID, E, G, I**). To further investigate the ascending aorta of ADAMTS5 deficient mice we used microscopic and histological studies to evaluate potential ascending aortic anomalies that may coincide with bicuspid aortic valves of the *Adamts5*$^{-/-}$;*Smad2*$^{+/-}$ (n=17) and large myxomatous valves of *Adamts5*$^{-/-}$ mice (n=19). All of both the *Adamts5*$^{-/-}$;*Smad2*$^{+/-}$ and *Adamts5*$^{-/-}$ mice had anomalies in their ascending aorta but the malformations varied and included: aortic stenosis, altered outflow tract (OFT) rotation, abnormal membranous interventricular septum, smooth muscle cell (SMC) loss, cell infiltration, abnormally thick aortic wall and altered geometry of the ascending aorta. Examples are shown of altered ascending aorta anomalies of a stenotic ascending aorta (Fig. 1B, F) and a lack of rotation of the aorta (Fig. 1C). Additional examples of anomalies are shown: loss of SMC (Fig. 1E, K, closed arrows) abnormal infiltration of cells (Fig. 1H, arrow), blood in the ascending aortic walls (Fig. 1G, I, J, K, L, open arrows).

However, the most penetrant anomaly was the increased thickness of the wall of the ascending aorta. This observation was further evaluated and demonstrated a statistically

significant increase in the width of the ascending aortic artery wall in both the double mutant *Adamts5*$^{-/-}$;*Smad2*$^{+/-}$ as well as the *Adamts5*$^{-/-}$ mice (Fig. 1J, Fig. 2). The box in the ascending aortic artery (Fig. 1A) was the region quantified and increased in wall thickness (Fig. 1A). Figure 2 shows the scoring of the combined aortic anomalies, as well as the penetrance of each aortic anomaly examined. The parentheses denote the penetrance in female (red) and male (blue) mice for each anomaly. While there is phenotypic variability in the anomalies and wall thickness of both *Adamts5*$^{-/-}$;*Smad2*$^{+/-}$ and *Adamts5*$^{-/-}$ mice, there is not a significant difference in penetrance between males and females.

The ADAMTS5 ECM substrate Acan was increased in adult Adamts5$^{-/-}$ mice and correlated with ascending aortic wall phenotypes

In order to decipher the primary role of ADAMTS5 in generating the ECM landscape of the aorta we have been examining its *in vivo* substrate Acan. We have observed that accumulation of Acan correlates with the aortic wall anomalies in young adult *Adamts5*$^{-/-}$ and *Adamts5*$^{-/-}$;*Smad2*$^{+/-}$ mice compared to wild type (Fig. 3B, C). High magnification of the aortic wall showed Acan accumulation near the intimal layer (Fig. 3E, F open arrow) and within the medial layer (Fig. 3E, F, closed arrows), which may contribute to the increased thickness of the ascending aorta in the *Adamts5*$^{-/-}$ mice and *Adamts5*$^{-/-}$;*Smad2*$^{+/-}$ mice. The localization of Acan in the ascending aortic wall was polarized, i.e. evident predominantly on the adventitial side of the smooth muscle cells in the medial layer (Fig. 3E, F, solid white arrows). Acan accumulation also correlated with altered elastic lamellae appearance (Fig. 3G–I, solid yellow arrows). Acan accumulation was quantified using IHC confocal images [16] (Fig. 3J) and Western blots from *Adamts5*$^{-/-}$ and littermates (n=8 each) (Fig. 3K, L). There was a significant increase in the two larger Acan band clusters at 270kD and 190kD, in the *Adamts5*$^{-/-}$ ascending aortas (Fig. 3K, L). There was also a reduction of the cleaved Acan fragment, neo-TEGE, (Fig. 3K, L) in the *Adamts5*$^{-/-}$ compared to *Adamts5*$^{+/+}$. These data suggest that in the *Adamts5*$^{-/-}$ and *Adamts5*$^{-/-}$ aorta, Acan accumulates and correlates with ascending aortic malformations i.e. aortopathies. Since the *Adamts5*$^{-/-}$ mice alone, without the heterozygous Smad2 allele, showed a highly penetrant aortic wall phenotype, we focused on the single mutant (*Adamts5*$^{-/-}$) in the subsequent analysis of this study to evaluate a potential molecular mechanism of altered aortic development, namely, altered Acan, an ECM substrate of ADAMTS5.

The onset of Acan accumulation in the Adamts5$^{-/-}$ aortic wall correlated with smooth muscle cell differentiation and elastic lamellae formation in vivo

To determine the developmental onset of Acan accumulation in the aorta, Acan IHC was performed on wild type and *Adamts5*$^{-/-}$ littermates (Fig. 4). In each developmental set, the *Adamts5*$^{-/-}$ ascending aorta had Acan immunolocalization that colocalized with αSMA, indicating that differentiating SMC of the developing aorta (and pulmonary artery) had more Acan associated in the *Adamts5*$^{-/-}$ compared to wild type (Fig. 4A–F). Acan accumulation was evident by embryonic day 14.5 (Fig. 4A, B). Shortly after birth, at postnatal day 7 (P7), the accumulation of Acan in *Adamts5*$^{-/-}$ mice, was predominantly on the left side of the ascending aortic wall, even though there was not yet a change in the geometry. The increase of Acan on the left side of the ascending aorta was observed in all ages of mice (Fig. 4D, solid arrow). However, when there was an abnormality in the aortic geometry, such as the

straight valvulosinus area observed in the *Adamts5*$^{-/-}$ at 1mo (Fig. 4F), Acan was less 'sided' but accumulated throughout the regions of the ascending aortic anomaly in *Adamts5*$^{-/-}$ mice. Quantification of the Acan confocal images at P7 revealed a significant increase in Acan in the *Adamts5*$^{-/-}$ ascending aorta compared to wild type (Fig. 4G). In addition, Western blot using the Acan core protein antibody also indicated a significant increase in 270kD Acan core protein in *Adamts5*$^{-/-}$ aortas compared to wild type (Fig. 4H, I). Collectively, these data indicate that after septation of the cardiac outflow tract in development, Acan accumulates in the ascending aortic wall of the *Adamts5*$^{-/-}$ mice and correlates with SMC differentiation and aortic abnormalities.

Immunolocalization of Neo-epitope antibodies that recognize the initial ADAMTS cleaved Acan fragments, neo-FREEE, neo-GLGS and neo-SSELE were increased in the developing Adamts5$^{-/-}$ aorta

Next, a series of neo-epitope antibodies were utilized that recognize the cleaved Acan fragments but not the intact molecule [23, 24]. An initial and prominent ADAMTS5 Acan cleavage site FREEE$_{1467}$↓$_{1468}$GLGSV, within the Chondroitin Sulfate binding domain 2 (CS2) of the Acan core protein, leaves neo-FREEE on the N-terminal fragment and neo-GLGS on the C terminal fragment, (Figure 9A). In the P7 *Adamts5*$^{-/-}$ aorta, the neo-FREEE and neo-GLGS had increased immunolocalization in the ascending wall compared with wild type (n= 4, Fig. 5A–H). The next and adjacent ADAMTS5 cleavage site SSELE$_{1279}$↓$_{1280}$GRGTI, recognized by neo-SSELE (Figure 9A; Fig.5I–L), was also increased in the *Adamts5*$^{-/-}$ ascending aorta (n=4). The immunolocalization of neo-FREEE, neo-GLGS and neo-SSELE were consistent with an ECM, or pericellular localization. Although it may seem counterintuitive that there was an increase in the neo-FREEE, neo-GLGS and neo SLEEE Acan fragments, these fragments are generated at the initial ADAMTS sites within the C terminal region of the Acan core protein. Western blots were performed on RIPA buffer lysates of 1 mo ascending aortic tissue from *Adamts5*$^{-/-}$ and wild type. There was an increase in the largest neo-GLGS fragment in the *Adamts5*$^{-/-}$ aortas with a corresponding reduction of the smaller sized fragment at 80kD (Fig. 5Q, R). Western blots using the neo-SSELE revealed significant increases in the 117kD and 65kD neo-SSELE fragments in the *Adamts5*$^{-/-}$ aortas compared to wild type. Of note, the Acan fragments, neo-FREEE, neo-GLGS and neo SSELE, were generated from a different ADAMTS family member other than ADAMTS5, potentially ADAMTS9 [25] in the *Adamts5*$^{-/-}$ aortas. However, the observation that these Acan fragments accumulated in the *Adamts5*$^{-/-}$ ascending aorta, indicates that ADAMTS5 is likely responsible for further degradation and cleavage of these Acan fragments, in wild type littermates. Thus, these initial Acan cleavage products appear more stable in the *Adamts5*$^{-/-}$ aortas that lack ADAMTS5, a highly efficient Acan protease.

Immunolocalization of Acan neo-TEGE, a highly digested interglobular domain Acan fragment was reduced in the developing Adamts5$^{-/-}$

However, examination of the Acan cleavage site TEGE$_{373}$↓$_{374}$ALGSV located near the N-terminus and within the interglobular domain (IGD) (**Table 1A**), using the Acan neo-TEGE antibody, was more prevalent in the wild type aorta (Fig. 5M–P). The neo-TEGE immunostaining appearing punctate and intracellular. Notably the Acan neo-TEGE antibody

recognizes a significantly more digested Acan core fragment, without the chondroitin sulfate domains, compared to neo-FREEE, neo-GLGS and neo-SSELE, that detect ADAMTS cleavage sites utilized at early stages of Acan turnover.

Mice with a mutation in the Acan ADAMTS cleavage site, TEGE$_{373}$↓$_{374}$ALGSV, exhibit a low penetrance of aortic wall defects

Since we observed differences in the Acan neo-TEGE immunolocalization in the *Adamts5*$^{-/-}$ ascending aorta, we wanted to determine if this ADAMTS Acan cleavage site was critical for ascending aortic wall development. Mice containing a mutation in the Acan TEGE$_{373}$↓$_{374}$ALGSV site, to TEGE$_{373}$↓$_{374}$NVYS termed 'Jaffa' that rendered this site non-cleavable [20], were examined. Mice with this mutation are viable and otherwise normal, exhibiting no alterations to cartilage or skeletal formation. Sulfation of Acan, indicative of the GAG side chain binding, is also normal in non-cleavable Acan Jaffa mice [20]. In comparison to the wild type littermates, two of the four Jaffa hearts examined exhibited minor aortic wall defects in the adventitia (Fig. 6N, O, arrows). Namely, the adventitia was not compacted and adjacent to the medial layer as observed in wild type mice. The adventitial staining of cleaved Acan fragments was also disrupted in *Adamts5*$^{-/-}$ mice. In addition, there were also abnormalities in the right ventricular myocardium at the base of the pulmonary artery in three out of the four Jaffa hearts examined (Fig. 6C–E, arrows). Although blocking the TEGE$_{373}$↓$_{374}$ALGSV cleavage site resulted in protection from Acan loss in cartilage erosion [20], mutation of this site resulted in a low penetrance of aortic adventitial defects in the cohort (n=4) of adult hearts from TEGE$_{373}$↓$_{374}$NVYS knock-in mice examined in this study (Fig. 6). Therefore, the ADAMTS Acan cleavage site, TEGE$_{373}$↓$_{374}$ALGSV may be important for normal aortic wall development, however it is likely that additional C terminal cleavage sites are also required since the aortic malformations in the Jaffa TEGE$_{373}$↓$_{374}$NVYS knock-in mice, were not as severe as in the *Adamts5*$^{-/-}$ mice.

Immunolocalization of Acan neo-DIPEN and neo-FFGVG, that result from cleavage within the interglobular domain, showed abnormal accumulation in the aortic media and associated with smooth muscle loss in the Adamts5$^{-/-}$ aorta

We also utilized Acan neo-epitope antibodies that bind to the DIPEN$_{341}$↓$_{342}$FFGVG site within the interglobular domain, near the N-terminus of Acan, that is also recognized by MMP proteases [26] (Fig. 9). In both P7 and adult, neo-DIPEN was prevalent in fibrous connective tissue rich regions, (i.e. the adventitia of the aorta and aortic valves) (Fig. 7). However, in the *Adamts5*$^{-/-}$ aorta there was increased immunolocalization of neo-DIPEN in the medial layer and associated with the smooth muscle cells (Fig. 7F, J white arrow). The abnormal localization of neo-DIPEN in the medial layer was accompanied by relatively less staining in the adventitial area, compared with wild type (Fig. 7J*). Thus, neo-DIPEN showed a differential localization pattern from wild type (Fig. 7I*). The neo-FFGVG antibody, which recognizes the C terminal fragment of the DIPEN$_{341}$↓$_{342}$FFGVG site, was also localized to the adventitia, cardiac valves (Fig. 8). The immunolocalization of neo-FFGVG, was similar to neo-DIPEN, and revealed abnormal localization of the Acan neo-FFGVG fragment to the medial layer in the *Adamts5*$^{-/-}$ aorta. Moreover, neo-FFGVG staining was enriched in the adventitia in the *Adamts5*$^{-/-}$ and associated with smooth muscle

cell loss within the medial layer (Fig. 8H, J, L, white arrows). Overall the neo-epitope Acan cleavage profiles exhibited a reproducibly altered pattern in the developing and adult *Adamts5*$^{-/-}$ aorta. In addition, the changes of neo-epitope-localized Acan cleavage fragments, were altered at different stages in the developing ascending aorta. The localization and intensity of staining of Acan and the different fragments detected by the neo-epitope Acan antibodies are summarized in Fig. 9.

Discussion

The contribution of ECM remodeling on cardiovascular development remains largely unexplored. Yet, changes in biomechanical forces on the heart, as the embryo grows, dictates the requirement for dramatic modifications in biomaterial properties of developing tissues, largely provided by the ECM architecture. Since mice deficient in the ECM protease ADAMTS5 with a concomitant reduction in Smad2 develop bicuspid aortic valves with high penetrance, [17] we initiated investigation to determine if these mice, like the human patient population, exhibit ascending aortic wall defects. We discovered a high penetrance of ascending aortic anomalies that included increased wall thickness, aortic stenosis and elastic lamellae fragmentation. The aortic anomalies in the *Adamts5*$^{-/-}$ mice correlated with accumulation of the ADAMTS5 substrate Acan. In tracing the developmental onset of the aortic wall anomalies in the *Adamts5*$^{-/-}$ aorta, Acan accumulated at the beginning of elastogenesis around E14.5. Initially this discovery was surprising given that Acan is predominantly a cartilage proteoglycan. However subsequent published reports emerged indicating massive accumulation of Acan is present in ruptured aortic tissue of thoracic aortic aneurysm patients, but not in healthy aortic tissue [10]. Reduction of ADAMTS5 in a murine model of atherosclerosis, was also published, revealing an increase in biglycan and versican [12]. In addition, a recent report by Suna et al indicated that the highest expression of *Adamts5*, *Vcan* and *Acan* was in the ascending region of the aortic artery, owing to the potential importance of Vcan and Acan turnover in this portion of the aortic artery [14]. However, the physiological role of Acan and its proteolytic cleavage by ADAMTS5 in the ascending aorta is not known.

In our effort to determine if the accumulation of Acan was a primary cause of the ascending aortopathies in the ADAMTS5 deficient mice, we examined the Acan cleaved fragments in the developing aortic tissue. Our hypothesis stated that Acan is efficiently turned over in elastic arterial tissue, since its detection has remained elusive until recent reports. Our results showed that shortly after birth in the *Adamts5*$^{-/-}$ aorta, localization of neo-epitope antibodies reproducibly indicated that the initial Acan ADAMTS cleavage fragments on the C terminal half of the core Acan protein were more prevalent in *Adamts5*$^{-/-}$ mice compared with wild type littermates. Since Acan cleavage initiates and progresses from the C-terminal end of the core protein we interpret these data to indicate that Acan cleavage fragments at the C-terminal region in the Acan core protein, are more stable in the context of ADAMTS5 deficiency in the developing aorta.

In addition, the N-terminal fragments, that represent a more highly digested Acan core, Acan neo-TEGE, were more prevalent in wild type mice in the ascending aorta shortly after birth. Mice containing a mutation in the NVTEGE$_{373}$↓$_{374}$ALGSV site, termed ‘Jaffa’ that

rendered this site non-cleavable, [20] had a partial penetrance of mild aortic wall anomalies, indicating that cleavage at this site in the Acan IGD domain may be important for arterial tissue, however other ADAMTS5 sites may play a more critical role. Neo-epitope antibodies that recognize a nearby Acan cleavage site denoted $DIPEN_{341}\downarrow_{342}FFGVG$, showed prominent staining, but altered localization in the ascending aorta of wild type compared to *Adamts5*$^{-/-}$ mice. Since these sites are both in the Acan IGD domain, these data may also implicate C-terminal ADAMTS5 cleavage sites likely play a role in Acan turnover in arterial tissue.

Given that high molecular weight Acan forms large complexes with hyaluronan, to provide rigid, non-compressible biomaterial properties to cartilage, its localization in arterial tissue which consists of a prevalence of cleaved Acan fragments, likely serves a dramatically different role in fibrous elastic tissue that allows expansion and contraction. These findings are consistent with reports that indicate aggrecanase activity is more apparent in tendon than cartilage. For example, greater than 65% of total Acan isolated from bovine tendon lacks the N-terminal G1 domain [27]. Acan fragments are also found in cultured tendon explants [27, 28]. Moreover, mice deficient in ADAMTS5 also exhibit loss of healing from tendinopathy that correlates with Acan accumulation enmeshed with cartilaginous-like cells [29]. In the postnatal heart, the N-terminal, smaller, cleaved Acan fragments (neo-FFGVG, neo-DIPEN) colocalized with fibrous connective tissue in the adventitia and cardiac valves; this pattern of localization was disrupted in the *Adamts5*$^{-/-}$ aorta where they colocalized with smooth muscle cell loss in the medial layer and abnormalities in the adventitia. It may be that the smaller or N-terminal cleaved Acan fragments play a role in collagen I matrix assembly in fibrous tissues. Changes in Acan were observed in vascular remodeling after injury, where there is a shift in ADAMTS gene expression and increased Acan synthesis, leading to increased Acan [14]. In ADAMTS5 deficient mice the tendinous and muscular tissues appear to be more sensitive to Acan accumulation than cartilage, since there is no defect in long bone formation with loss of ADAMTS5 [30]. In cartilage tissue ADAMTS5 deficiency does not block Acan cleavage, perhaps due to the presence and upregulation of ADAMTS9 [31]. Therefore, the context of Acan and ADAMTS5 expression yields different results owing to the complexity of protease-substrate interactions required to achieve diverse biomaterial properties in many types of connective tissues [32].

In addition to Acan, ADAMTS5 has additional proteoglycan substrates of the lectican class, that may contribute to the ascending aortic defects of *Adamts5*$^{-/-}$ mice. An important proteomic study was performed by Mayr and colleagues in which they examined the proteolytic profile of the ascending aorta in *Adamts5*$^{-/-}$ and wild type mice challenged with Angiotensin II; the aortic tissue from *Adamts5*$^{-/-}$ mice exhibited significantly more Vcan than wild type mice [15]. When exogenous ADAMTS5 is added to wild type aortic tissue; Vcan and Acan were released at a significant level from the aortic tissue indicating the initial report of Acan susceptibility to ADAMTS5-mediated cleavage in arterial tissue [12]. In addition, Vcan cleaved fragment, Versikine was significantly reduced in the aortas of *Adamts5*$^{-/-}$ mice [15]. In vessel wounding experiments Vcan accumulates and there is a shift in ADAMTS expression, indicating that similar to Angiotensin II challenge, ADAMTS5-mediated Vcan cleavage is highly relevant to arterial wall remodeling [33–39]. Neurocan and Brevican are additional substrates of ADAMTS5 with predominant expression in neural

tissues, that have not been reported in ascending aortic tissue [30]. As additional investigative neo-epitope antibodies and cleavage resistant proteoglycan ADAMTS substrate models become available, the contribution of ADAMTS derived proteoglycan cleavage will be further elucidated in the ascending aorta.

A distinct role for the ADAMTS cleaved proteoglycan fragments compared to the larger more intact forms has been noted for both Acan and Vcan. The N-terminal fragment of Vcan, coined Versikine, elicits apoptosis during digit formation, a distinct role from the intact core proteoglycan [19]. Reports also indicate that a small Acan N-terminal ADAMTS-MMP fragment, 32 mer, contributes to inflammation in osteoarthritis and exacerbates disease progression [40]. In addition to proteolytic cleavage, proteoglycan substrates of ADAMTS5 generate heterogeneity though differential splicing. Thus, we have scratched the surface of proteome complexity generated by protease-substrate interactions in ADAMTS5-mediated ECM remodeling in the ascending aorta.

Use of mice that show a reproducible phenotype for myxomatous valves and ascending aortic anomalies may be helpful to elucidate mechanisms of etiologies that contribute to aortic aneurysms in humans, although to date, no animal model recapitulates human aneurysmal disease. Here we show that the development of the aorta in ADAMTS5 mice exhibits alterations in Acan cleavage neo-epitopes that correlate with valve and ascending wall anomalies. Recent reports on aneurysmal aortic wall tissue from human patients exhibited Acan accumulation, but the use of end-stage diseased tissues makes it challenging to determine the origin of the pathology. Perhaps slight developmental anomalies of ECM processing of proteoglycans such as Acan, together with the altered flow, caused by the larger aortic and pulmonary valves contributes to aortic aneurysmal progression in humans. Therefore, further investigation using animal models devoid of ADAMTS5, with reproducible aortic phenotypes, may elucidate novel therapeutics to treat ascending aortic aneurysms and diagnostic approaches to better predict disease progression that requires surgical intervention. This study is another example of how mouse models, deficient in ECM proteases, can be utilized to better understand the subset of the proteome that involves proteases and their substrates, referred to as the degradome. Moreover, the mechanism of ADAMTS mediated ECM remodeling may emerge as a key element in regenerative medicine approaches due to its physiological requirement in mammalian development.

Supplementary Material

Refer to Web version on PubMed Central for supplementary material.

Acknowledgments

Sources of Funding: American Heart Association #17GRNT33700214 (CBK), NIH, NHLBI HL121382 (CBK), T32 DE017551 (AR, SCP), R25HL096316 (BH).

Non-standard abbreviations and acronyms

ECM	extracellular matrix

ADAMTS5 A Disintegrin-like and Metalloprotease domain with ThromboSpondin type motifs

References

1. Clouse WD, Hallett JW Jr., Schaff HV, Spittell PC, Rowland CM, Ilstrup DM, Melton LJ 3rd. Acute aortic dissection: Population-based incidence compared with degenerative aortic aneurysm rupture. Mayo Clin Proc. 2004;79:176–180 [PubMed: 14959911]
2. LeMaire SA, Russell L. Epidemiology of thoracic aortic dissection. Nat Rev Cardiol. 2011;8:103–113 [PubMed: 21173794]
3. Hadler-Olsen E, Fadnes B, Sylte I, Uhlin-Hansen L, Winberg JO. Regulation of matrix metalloproteinase activity in health and disease. The FEBS journal. 2011;278:28–45 [PubMed: 21087458]
4. Lu H, Aikawa M. Many faces of matrix metalloproteinases in aortic aneurysms. Arterioscler Thromb Vasc Biol. 2015;35:752–754 [PubMed: 25810296]
5. Kadoglou NP, Liapis CD. Matrix metalloproteinases: Contribution to pathogenesis, diagnosis, surveillance and treatment of abdominal aortic aneurysms. Current medical research and opinion. 2004;20:419–432 [PubMed: 15119978]
6. Longo GM, Xiong W, Greiner TC, Zhao Y, Fiotti N, Baxter BT. Matrix metalloproteinases 2 and 9 work in concert to produce aortic aneurysms. J Clin Invest. 2002;110:625–632 [PubMed: 12208863]
7. Pyo R, Lee JK, Shipley JM, Curci JA, Mao D, Ziporin SJ, Ennis TL, Shapiro SD, Senior RM, Thompson RW. Targeted gene disruption of matrix metalloproteinase-9 (gelatinase b) suppresses development of experimental abdominal aortic aneurysms. J Clin Invest. 2000;105:1641–1649 [PubMed: 10841523]
8. Oller J, Mendez-Barbero N, Ruiz EJ, Villahoz S, Renard M, Canelas LI, Briones AM, Alberca R, Lozano-Vidal N, Hurle MA, Milewicz D, Evangelista A, Salaices M, Nistal JF, Jimenez-Borreguero LJ, De Backer J, Campanero MR, Redondo JM. Nitric oxide mediates aortic disease in mice deficient in the metalloprotease adamts1 and in a mouse model of marfan syndrome. Nat Med. 2017;23:200–212 [PubMed: 28067899]
9. Ren P, Hughes M, Krishnamoorthy S, Zou S, Zhang L, Wu D, Zhang C, Curci JA, Coselli JS, Milewicz DM, LeMaire SA, Shen YH. Critical role of adamts-4 in the development of sporadic aortic aneurysm and dissection in mice. Scientific reports. 2017;7:12351 [PubMed: 28955046]
10. Cikach FS, Koch CD, Mead TJ, Galatioto J, Willard BB, Emerton KB, Eagleton MJ, Blackstone EH, Ramirez F, Roselli EE, Apte SS. Massive aggrecan and versican accumulation in thoracic aortic aneurysm and dissection. JCI Insight. 2018;3
11. Apte SS. A disintegrin-like and metalloprotease (reprolysin-type) with thrombospondin type 1 motif (adamts) superfamily-functions and mechanisms. J Biol Chem. 2009
12. Didangelos A, Mayr U, Monaco C, Mayr M. Novel role of adamts-5 protein in proteoglycan turnover and lipoprotein retention in atherosclerosis. J Biol Chem. 2012;287:19341–19345 [PubMed: 22493487]
13. Wang K, Xu J, Hunter DJ, Ding C. Investigational drugs for the treatment of osteoarthritis. Expert opinion on investigational drugs. 2015:1–18
14. Suna G, Wojakowski W, Lynch M, Barallobre-Barreiro J, Yin X, Mayr U, Baig F, Lu R, Fava M, Hayward R, Molenaar C, White SJ, Roleder T, Milewski KP, Gasior P, Buszman PP, Buszman P, Jahangiri M, Shanahan CM, Hill J, Mayr M. Extracellular matrix proteomics reveals interplay of aggrecan and aggrecanases in vascular remodeling of stented coronary arteries. Circulation. 2018;137:166–183 [PubMed: 29030347]
15. Fava M, Barallobre-Barreiro J, Mayr U, Lu R, Didangelos A, Baig F, Lynch M, Catibog N, Joshi A, Barwari T, Yin X, Jahangiri M, Mayr M. Role of adamts-5 in aortic dilatation and extracellular matrix remodeling. Arterioscler Thromb Vasc Biol. 2018;38:1537–1548 [PubMed: 29622560]
16. Dupuis LE, McCulloch DR, McGarity JD, Bahan A, Wessels A, Weber D, Diminich AM, Nelson CM, Apte SS, Kern CB. Altered versican cleavage in adamts5 deficient mice; a novel etiology of myxomatous valve disease. Dev Biol. 2011;357:152–164 [PubMed: 21749862]

17. Dupuis LE, Osinska H, Weinstein MB, Hinton RB, Kern CB. Insufficient versican cleavage and smad2 phosphorylation results in bicuspid aortic and pulmonary valves. J Mol Cell Cardiol. 2013;60:50–59 [PubMed: 23531444]
18. Jungers KA, Le Goff C, Somerville RP, Apte SS. Adamts9 is widely expressed during mouse embryo development. Gene Expr Patterns. 2005;5:609–617 [PubMed: 15939373]
19. McCulloch DR, Nelson CM, Dixon LJ, Silver DL, Wylie JD, Lindner V, Sasaki T, Cooley MA, Argraves WS, Apte SS. Adamts metalloproteases generate active versican fragments that regulate interdigital web regression. Dev Cell. 2009;17:687–698 [PubMed: 19922873]
20. Little CB, Meeker CT, Golub SB, Lawlor KE, Farmer PJ, Smith SM, Fosang AJ. Blocking aggrecanase cleavage in the aggrecan interglobular domain abrogates cartilage erosion and promotes cartilage repair. J Clin Invest. 2007;117:1627–1636 [PubMed: 17510707]
21. Kern CB, Norris RA, Thompson RP, Argraves WS, Fairey SE, Reyes L, Hoffman S, Markwald RR, Mjaatvedt CH. Versican proteolysis mediates myocardial regression during outflow tract development. Dev Dyn. 2007;236:671–683 [PubMed: 17226818]
22. Rogers AW, Cisewski SE, Kern CB. The zonal architecture of the mandibular condyle requires adamts5. J Dent Res. 2018;97:1383–1390 [PubMed: 29879379]
23. Fosang AJ, Last K, Gardiner P, Jackson DC, Brown L. Development of a cleavage-site-specific monoclonal antibody for detecting metalloproteinase-derived aggrecan fragments: Detection of fragments in human synovial fluids. The Biochemical journal. 1995;310 (Pt 1):337–343 [PubMed: 7544117]
24. Fosang AJ, Last K, Stanton H, Golub SB, Little CB, Brown L, Jackson DC. Neoepitope antibodies against mmp-cleaved and aggrecanase-cleaved aggrecan. Methods Mol Biol. 2010;622:312–347 [PubMed: 20135291]
25. Kern CB, Wessels A, McGarity J, Dixon LJ, Alston E, Argraves WS, Geeting D, Nelson CM, Menick DR, Apte SS. Reduced versican cleavage due to adamts9 haploinsufficiency is associated with cardiac and aortic anomalies. Matrix Biol. 2010;29:304–316 [PubMed: 20096780]
26. Fosang AJ, Neame PJ, Hardingham TE, Murphy G, Hamilton JA. Cleavage of cartilage proteoglycan between g1 and g2 domains by stromelysins. J Biol Chem. 1991;266:15579–15582 [PubMed: 1874716]
27. Samiric T, Ilic MZ, Handley CJ. Characterisation of proteoglycans and their catabolic products in tendon and explant cultures of tendon. Matrix Biol. 2004;23:127–140 [PubMed: 15246111]
28. Rees SG, Flannery CR, Little CB, Hughes CE, Caterson B, Dent CM. Catabolism of aggrecan, decorin and biglycan in tendon. The Biochemical journal. 2000;350 Pt 1:181–188 [PubMed: 10926842]
29. Bell R, Li J, Shewman EF, Galante JO, Cole BJ, Bach BR Jr., Troy KL, Mikecz K, Sandy JD, Plaas AH, Wang VM. Adamts5 is required for biomechanically-stimulated healing of murine tendinopathy. Journal of orthopaedic research : official publication of the Orthopaedic Research Society. 2013;31:1540–1548 [PubMed: 23754494]
30. Stanton H, Melrose J, Little CB, Fosang AJ. Proteoglycan degradation by the adamts family of proteinases. Biochim Biophys Acta. 2011;1812:1616–1629 [PubMed: 21914474]
31. Rogerson FM, Last K, Golub SB, Gauci SJ, Stanton H, Bell KM, Fosang AJ. Adamts-9 in mouse cartilage has aggrecanase activity that is distinct from adamts-4 and adamts-5. International journal of molecular sciences. 2019;20
32. East CJ, Stanton H, Golub SB, Rogerson FM, Fosang AJ. Adamts-5 deficiency does not block aggrecanolysis at preferred cleavage sites in the chondroitin sulfate-rich region of aggrecan. J Biol Chem. 2007;282:8632–8640 [PubMed: 17255106]
33. Kenagy RD, Plaas AH, Wight TN. Versican degradation and vascular disease. Trends in cardiovascular medicine. 2006;16:209–215 [PubMed: 16839865]
34. Merrilees MJ, Ching PS, Beaumont B, Hinek A, Wight TN, Black PN. Changes in elastin, elastin binding protein and versican in alveoli in chronic obstructive pulmonary disease. Respir Res. 2008;9:41 [PubMed: 18485243]
35. Sandy JD, Westling J, Kenagy RD, Iruela-Arispe ML, Verscharen C, Rodriguez-Mazaneque JC, Zimmermann DR, Lemire JM, Fischer JW, Wight TN, Clowes AW. Versican v1 proteolysis in

human aorta in vivo occurs at the glu441-ala442 bond, a site that is cleaved by recombinant adamts-1 and adamts-4. J Biol Chem. 2001;276:13372–13378. [PubMed: 11278559]

36. Wight TN. Versican: A versatile extracellular matrix proteoglycan in cell biology. Curr Opin Cell Biol. 2002;14:617–623 [PubMed: 12231358]
37. Wight TN. Arterial remodeling in vascular disease: A key role for hyaluronan and versican. Front Biosci. 2008;13:4933–4937 [PubMed: 18508558]
38. Wight TN, Lara S, Riessen R, Le Baron R, Isner J. Selective deposits of versican in the extracellular matrix of restenotic lesions from human peripheral arteries. American Journal of Pathology. 1997;151:963–973 [PubMed: 9327730]
39. Yao LY, Moody C, Schonherr E, Wight TN, Sandell LJ. Identification of the proteoglycan versican in aorta and smooth muscle cells by DNA sequence analysis, in situ hybridization and immunohistochemistry. Matrix Biology. 1994;14:213–225 [PubMed: 7921538]
40. Lees S, Golub SB, Last K, Zeng W, Jackson DC, Sutton P, Fosang AJ. Bioactivity in an aggrecan 32-mer fragment is mediated via toll-like receptor 2. Arthritis Rheumatol. 2015;67:1240–1249 [PubMed: 25707860]

Highlights

Mice deficient in the extracellular matrix protease ADAMTS5 exhibit a high penetrance of ascending aortic wall defects.

The developing ascending aortic wall from ADAMTS5 deficient mice exhibits altered proteolytic cleavage of its proteoglycan substrate aggrecan.

ADAMTS5 mediated aggrecan cleavage may be an essential mechanism for aortic wall development.

Altered ADAMTS5 mediated proteoglycan remodeling may contribute to bicuspid aortic valves with accompanying ascending aortic anomalies.

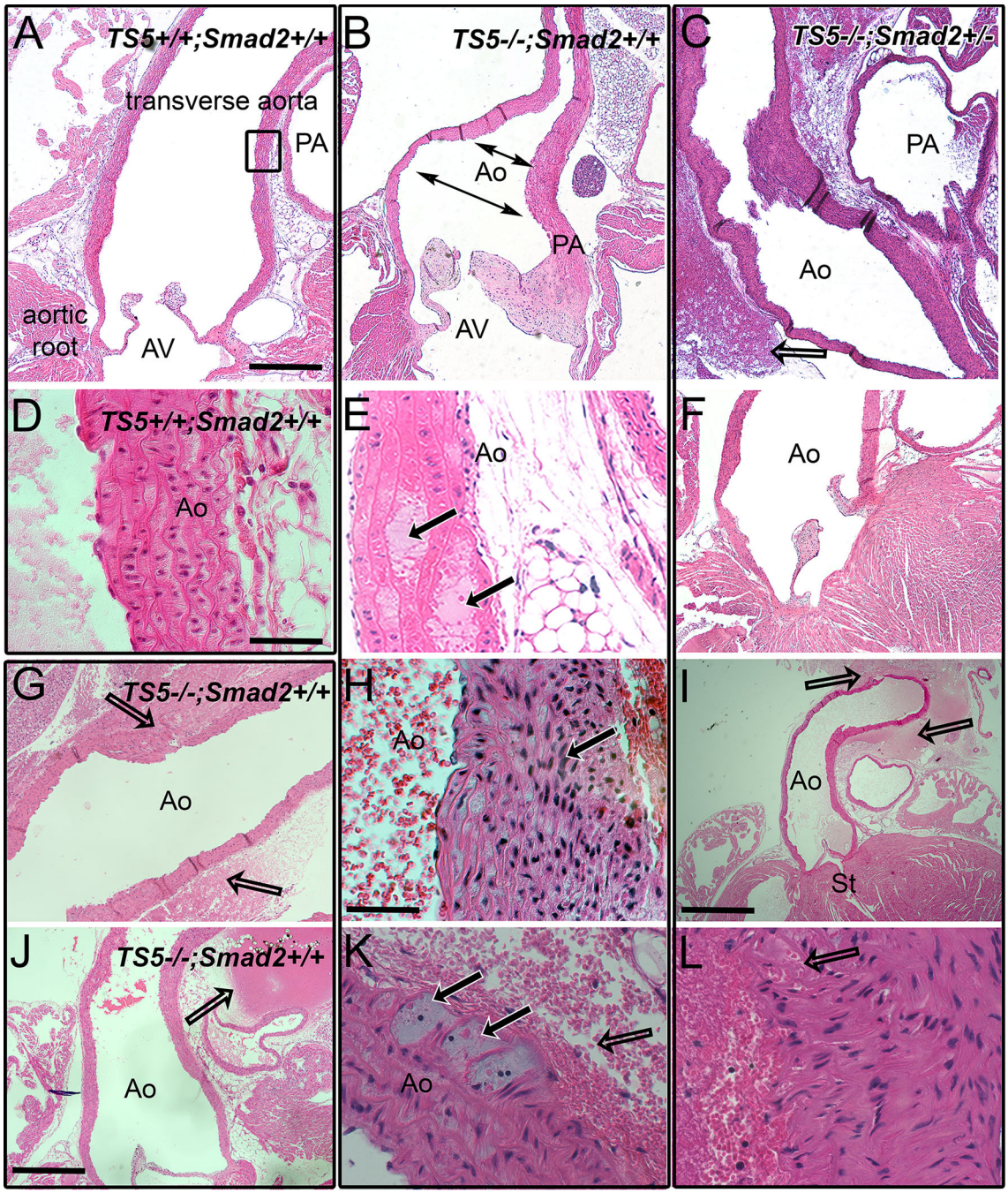

Figure 1: Mice deficient in the ADAMTS5 protease exhibit ascending aortic anomalies.

Histological sections of adult wild type (*TS5*$^{+/+}$*; Smad2*$^{+/+}$, A, D), ADAMTS5 deficient (*TS5*$^{-/-}$*; Smad2*$^{+/+}$, B, E, G, H, J, K) and ADAMTS5 deficient, heterozygous in the Smad2 allele, (*TS5*$^{-/-}$*; Smad2*$^{+/-}$, C, F, I, L) are depicted. Geometry of the transverse, ascending aorta in wild type mice (A) with altered geometry in ADAMTS5 deficiency (B, double-headed arrows) and a loss of appropriate rotation in the *TS5*$^{-/-}$*; Smad2*$^{+/-}$, that further contributes to defects in the ascending aorta that correlate with ADAMTS5 deficiency. Examples of altered cellularity (E, H, K, closed arrows). Blood cells in the aortic medial

layer, breaks in the aortic wall and (G, I, J, K, L, open arrows) consistent with aortic dissection. Bar in A=250μm applies to B, C, F, G; bar in D= 50μm, applies to E, H, K, L; I = 500μm; J=350μm.`

Genotype	Stenotic	OFT Rotation	Membranous IVS	SMC loss/Cell Infiltration	RBC in Ao wall	*Thick Aortic Wall	Aortic Geometry	Combined Aortic Anomalies
TS5+/+;Smad2+/+	0/11	1/11	0/11	0/11	0/11	0/11	0/11	**1/11 (7, 4)**
TS5 -/-;Smad2+/+								
Tricuspid	8/18	7/18	1/18	4/18	7/18	7/18	14/18	11/18
Bicuspid	1/1	0/1	0/1	0/1	0/1	1/1	1/1	1/1
Total	(5, 4) 9/19	(4, 3) 7/19	(0,1) 1/19	(3, 1) 4/19	(6, 1) 7/19	(7, 8) 15/19	(6, 6) 12/19	**19/19 (9, 10)**
TS5-/-; Smad2+/-								
Tricuspid	6/10	6/10	2/10	2/10	5/10	10/10	5/10	10/10
Bicuspid	2/7	1/7	4/7	3/7	3/7	5/7	5/7	7/7
Total	(4, 4) 8/17	(4, 3) 7/17	(3, 3) 6/17	(3, 2) 5/17	(5, 3) 8/17	(8, 7) 15/17	(5, 5) 10/17	**17/17 (8, 9)**
TS5+/+;Smad2+/-	0/4	0/4	0/4	0/4	0/4	0/4	0/4	**0/4 (2, 2)**

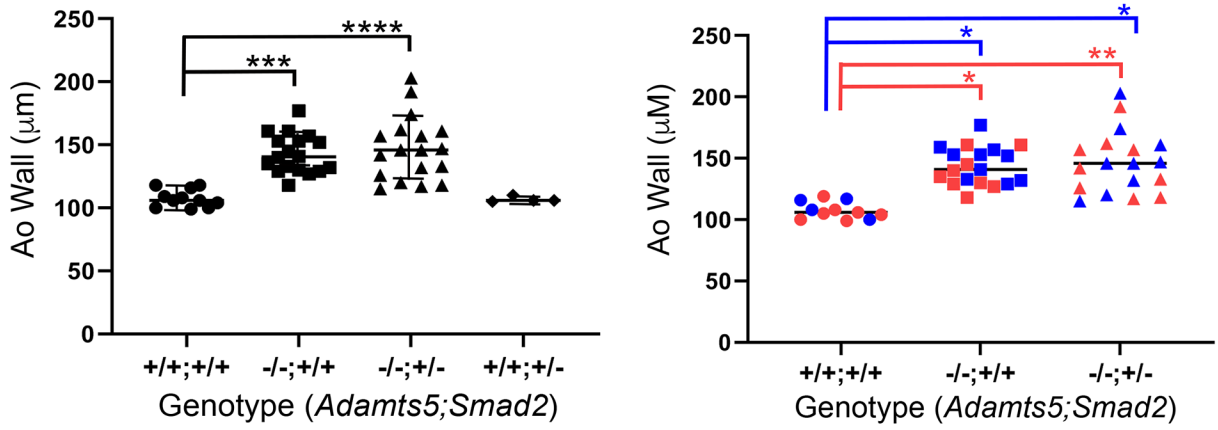

Figure 2: Mice deficient in the extracellular matrix protease, ADAMTS5, display a constellation of outflow tract related anomalies related to the ascending aorta.

Ascending aortic anomalies are scored for the following genotypes: wild type, *Adamts5*$^{+/+}$ (*TS5*$^{+/+}$;*Smad2*$^{+/+}$, n=11), *Adamts5*$^{-/-}$ (*TS5*$^{-/-}$;*Smad2*$^{+/+}$, n=19) and *Adamts5*$^{-/-}$;*Smad2*$^{+/-}$ (*TS5*$^{-/-}$;*Smad2*$^{+/+}$, n=17) with a high penetrance of bicuspid aortic valves, as well as control mice (*TS5*$^{+/+}$;*Smad2*$^{+/-}$). Stenosis at the opening of the left ventricle and aortic root, outflow tract (OFT) rotation, membranous interventricular septum (IVS), smooth muscle cell (SMC) loss, or infiltration into the aortic (Ao) wall, red blood cells (RBC) in or around the aortic wall consistent with aortic dissection, *thick aortic wall, quantified in graphs below, and altered aortic geometry. Penetrance is indicated in the 'Total' for each anomaly. Penetrance of female (red) and male (blue) is noted to the left of the total of each anomaly examined. The red/blue sex representations of the total examined are noted on the right side of the bold values in the far-right column. Horizontal lines in the graph represent the combined mean, with the error bars representing the standard deviation of the mean. Graphs denote the quantification of the aortic wall thickness with female and male mice combined, then followed by the separation of the sexes (red-female, blue-male) in the right graph. Statistically significant experimental parameters are indicated: *P<0.05; **P<0.01; ***P<0.001, **** P<0.0001.

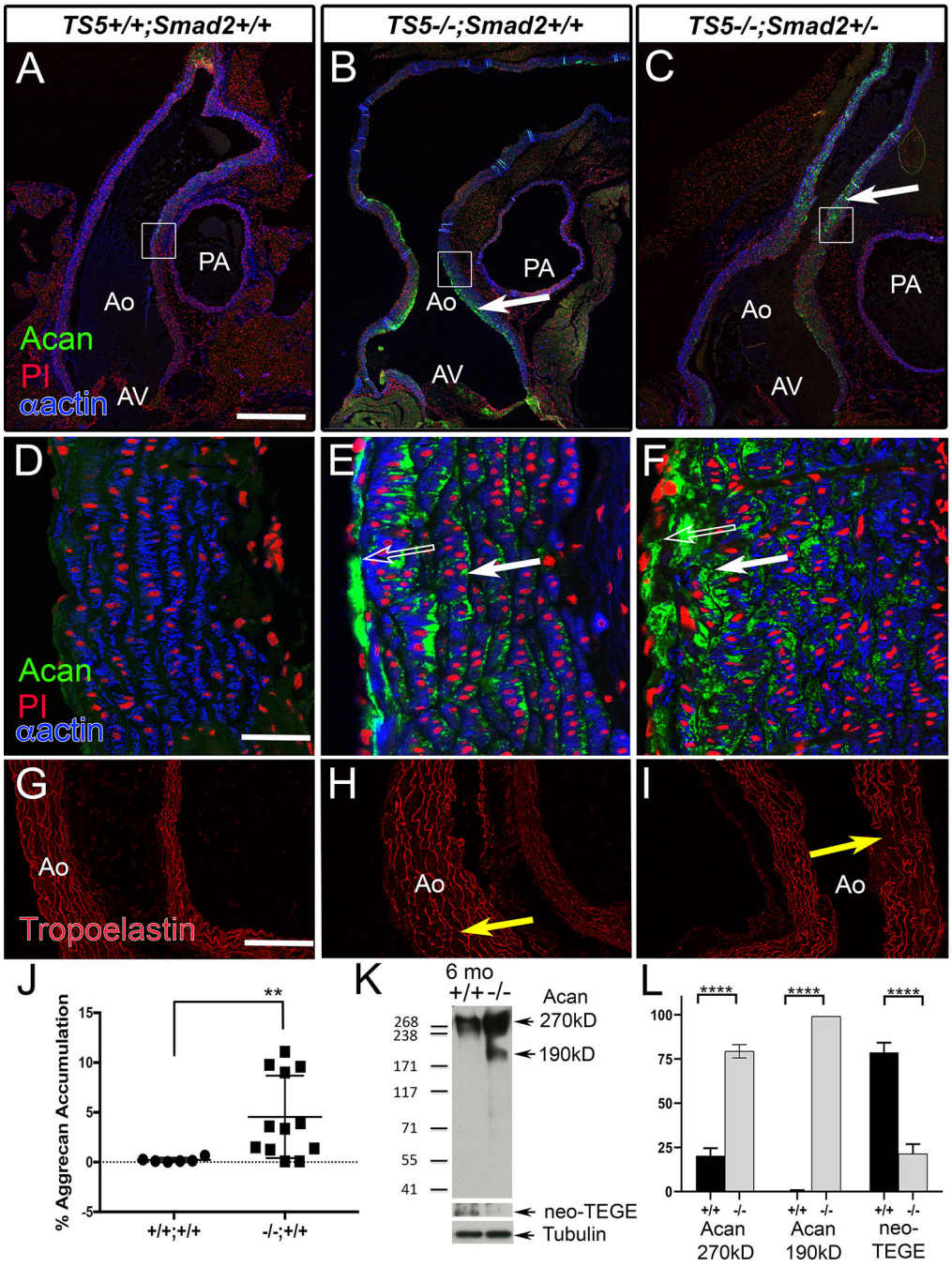

Figure 3: Ascending aortic anomalies correlate with aggrecan accumulation in the *Adamts5*$^{-/-}$ deficient mice.

Histological sections of adult wild type (*TS5*$^{+/+}$*; Smad2*$^{+/+}$, A, D, G), ADAMTS5 deficient (*TS5*$^{-/-}$*; Smad2*$^{+/+}$, B, E, H) and ADAMTS5 deficient, heterozygous in the Smad2 allele, (*TS5*$^{-/-}$*; Smad2*$^{+/-}$, C, F, I) are shown. Geometry of the transverse, ascending aorta in wild type mice (A) with altered geometry in ADAMTS5 deficiency (B, C, white arrows). Acan localization (green) correlates with aortic anomalies (B, C, white arrows). Boxes in A-C magnified in D-F. Open arrows, endothelial Acan, closed arrows-medial layer Acan. Blue- α smooth muscle actin; red-propidium iodide (A-F). Tropoelastin staining (G, H, I, red) to

highlight elastic lamellae fragmentation (H, I, yellow arrows). Quantification of % Acan accumulation from confocal Immunohistological images (J). Western blot of 'intact' Acan and reduction of neo-TEGE, N-terminal Acan fragment in adult *Adamts5*$^{-/-}$ aortas (K). Quantification of Western Acan and neo-TEGE of Adult *Adamts5*$^{+/+}$ (+/+) and *Adamts5*$^{-/-}$ (−/−) in L. Bar in A=200μm applies to B, C; bar in D= 50μm, applies to E-I. ** $P<0.01$; **** $P<0.0001$.

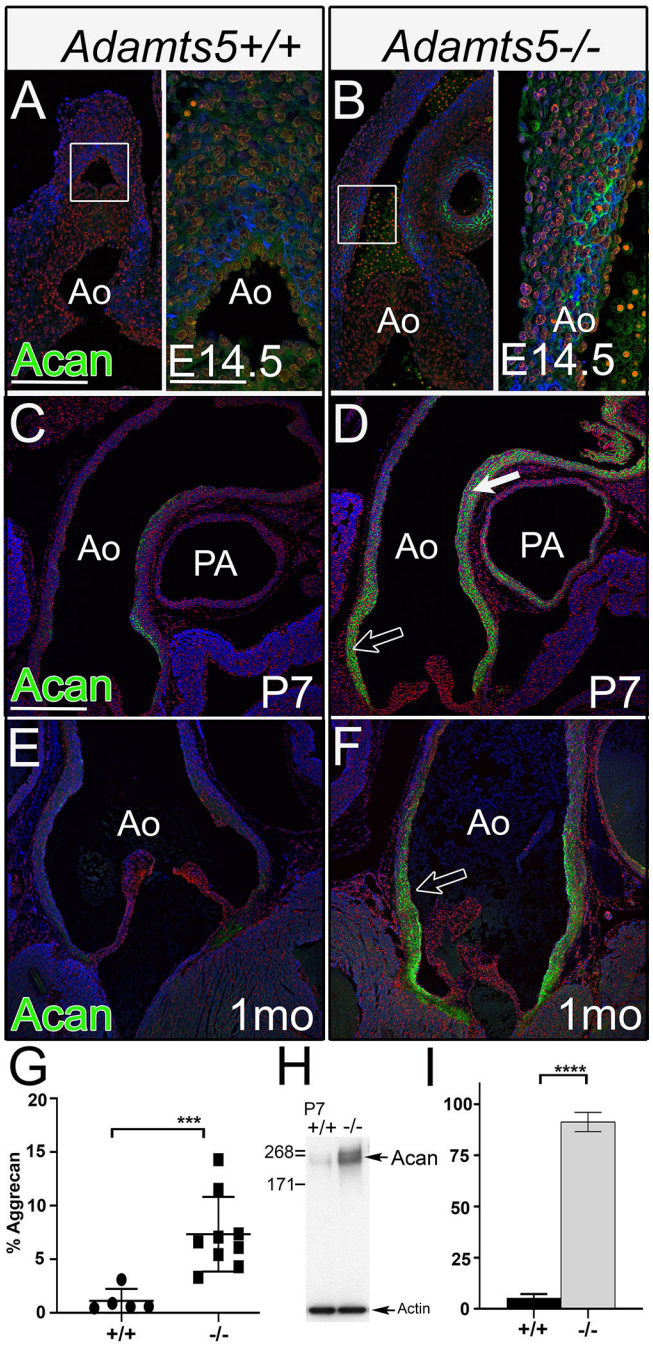

Figure 4: Developmental aggrecan accumulation correlates with elastic lamellae formation at embryonic day 14.5.

Histological sections of *Adamts5*$^{+/+}$ (A, C, E), and *Adamts5*$^{-/-}$ (B, D, F) are shown. Immunolocalization of Acan (green) blue- α smooth muscle actin (αSMA); red-propidium iodide (PI), (A-F). Boxes in A, B, increased in magnification right panel to show overlap of Acan, and αSMA. Open arrow, increased Acan staining in the valvulosinus. Solid arrow (D) increased Acan on the left side of the Ao in *Adamts5*$^{-/-}$ hearts. Quantification of confocal images of postnatal day 7 (P7) Acan immunohistochemistry (G). Western blot of Acan

accumulation at P7 (H). Quantification of Western (I). Bar in A=100μm applies to B; bar in C= 100μm, applies to D-F. ***P<0.001, **** P<0.0001.

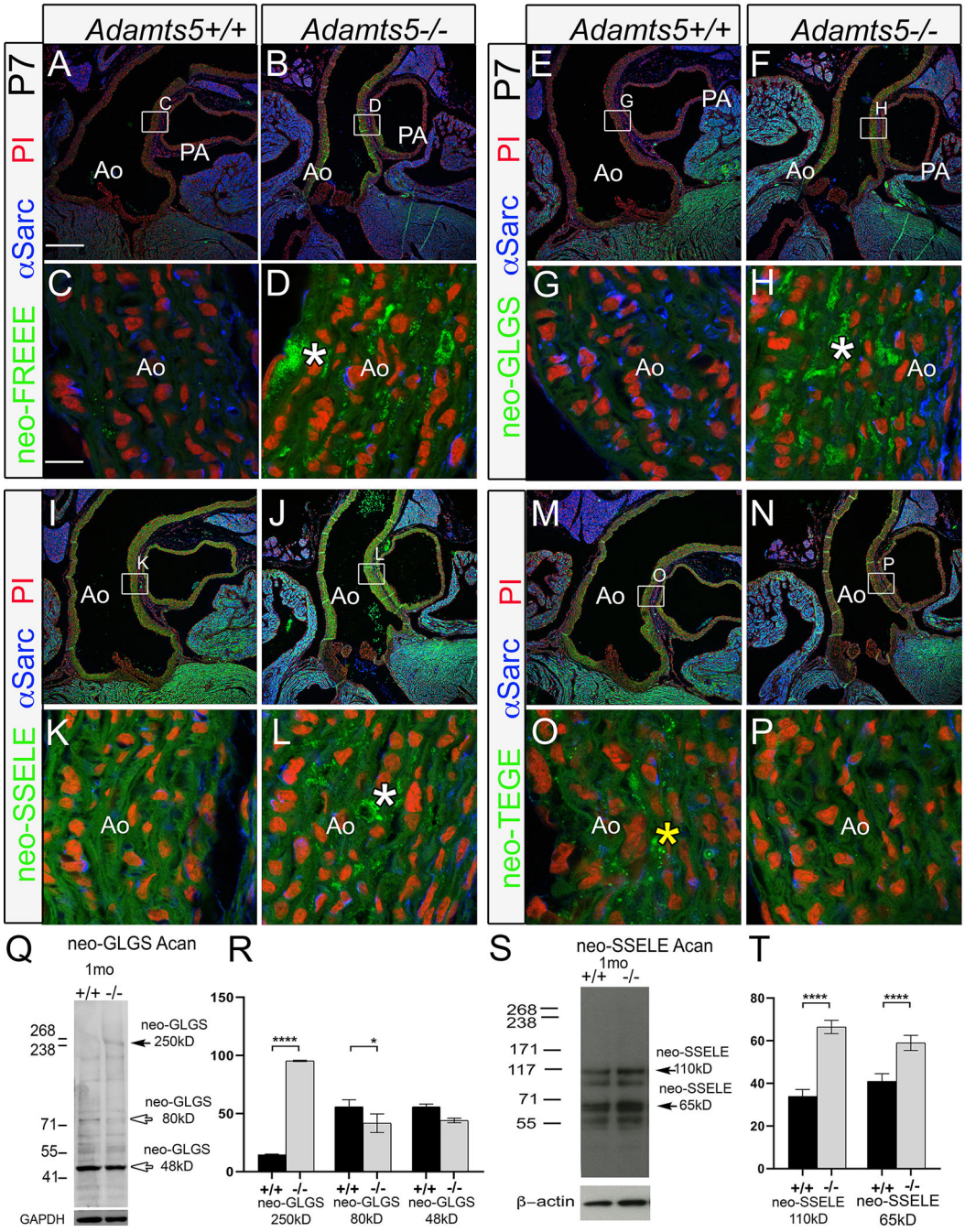

Figure 5: Aggrecan neo-epitope antibodies, that detect cleaved Acan fragments, exhibit differential immunolocalization in the *Adamts5*$^{-/-}$ ascending aorta at postnatal day 7.

Histological sections of *Adamts5*$^{+/+}$ (A, C, E, G, I, K, M, O), and *Adamts5*$^{-/-}$ (B, D, F, H, J, L, N, P). Boxes in A, B, E, F, I, J, M, N, magnified in C, D, G, H, K, L, O, P respectively. Immunolocalization of Acan neo-FREEE (A-D, green), Acan neo-GLGS (E-H, green), Acan neo-SSELE (I-L, green), Acan neo-TEGE Acan (M-P, green); blue- α smooth muscle actin (αSMA); red-propidium iodide (PI). White asterisk-increased localization of initial C-terminal neo-Acan fragments in *Adamts5*$^{-/-}$ (B, D, F, H, J, L). Yellow asterisk (O) increased localization of the Acan neo-TEGE fragment in the IGD domain in the N-terminal Acan

region that is more prevalent in *Adamts5*$^{+/+}$ (O). Ao-aorta, PA-pulmonary artery. Western blot of neo-GLGS from lysates of 1 mo *Adamts5*$^{-/-}$ aortas (Q). Quantification of Western neo-GLGS *Adamts5*$^{+/+}$ (+/+) and *Adamts5*$^{-/-}$ (−/−) in R. Western blot of neo-SSELE from lysates of 1 mo *Adamts5*$^{-/-}$ aortas (S). Quantification of Western neo-SSELE *Adamts5*$^{+/+}$ (+/+) and *Adamts5*$^{-/-}$ (−/−) in T. Bar in A=200μm applies to B, E, F, I, J, M, N; bar in C= 50μm, applies to D, G, H, K, L, O, P. **P*<0.05; **** *P*<0.0001.

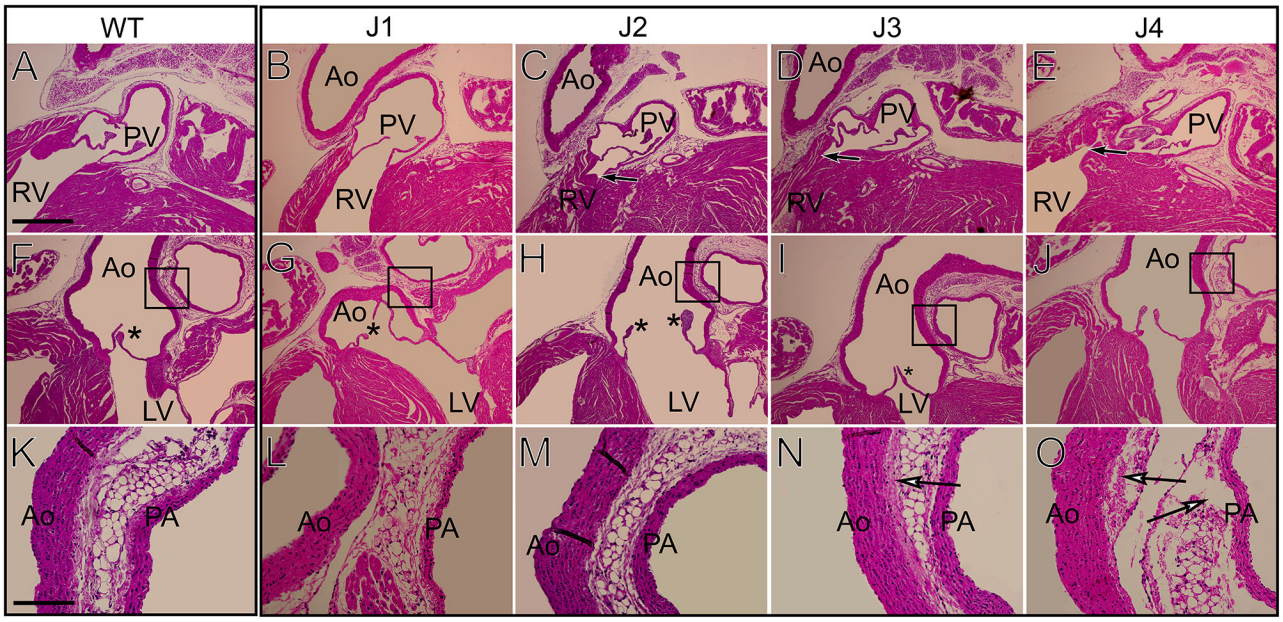

Figure 6: Mice containing a mutation in the aggrecan ADAMTS cleavage site NVTEGE$_{373}$↓$_{374}$ALGSV, termed 'Jaffa', exhibit a low penetrance of aortic wall defects.

Histological sections of adult wild type (WT, A, F, K) and Jaffa (B-E, G-J, L-O), mice. Frontal sections of the pulmonary valve (PV) and pulmonary artery (A-E), the ascending aorta (Ao) and aortic valves (denoted by asterisks in F-J). Arrows in C-E indicate stenotic RV, not found in WT. Open arrows (O) show abnormal adventitia in aortic and pulmonary artery. Boxes in F-J, increased in magnification in K-O respectively to highlight the ascending aortic wall. RV-right ventricle; LV-left ventricle. Bar in A=250μm applies to B, C; bar in D= 100μm, applies to E-I.

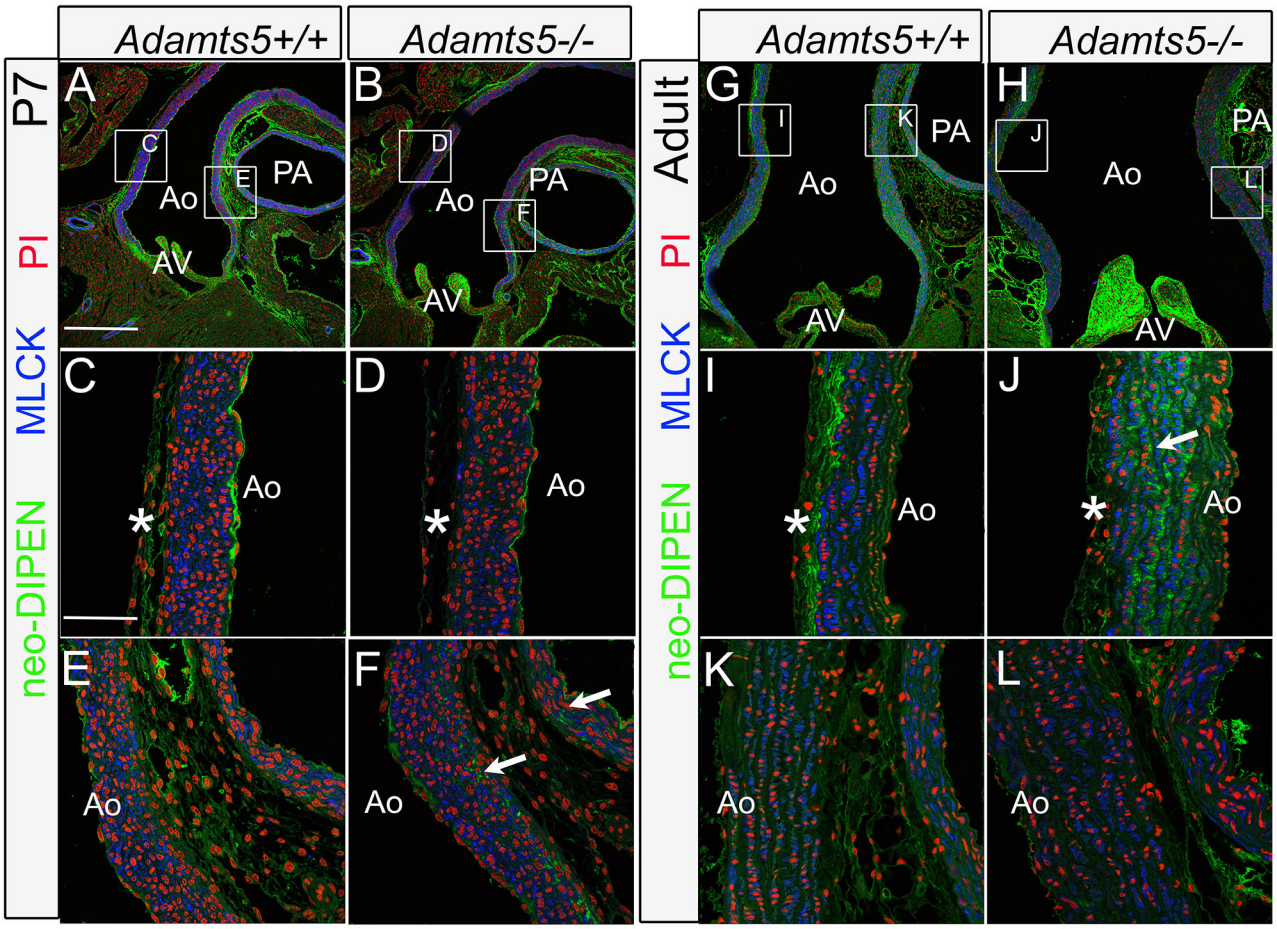

Figure 7: Aggrecan neo-epitope antibody neo-DIPEN exhibits a differential pattern of expression in the ascending aorta of postnatal day 7 and adult *Adamts5*$^{-/-}$ mice.

Histological sections of *Adamts5*$^{+/+}$ hearts (A, C, E, G, I, K), and *Adamts5*$^{-/-}$ hearts (B, D, F, H, J, L). Boxes in A, magnified in C, E; boxes in B, magnified in D, F; boxes in G, magnified in I, K; boxes in H, magnified in J, L. Immunolocalization of Acan neo-DIPEN (A-L, green), at postnatal day 7 (P7, A-F) and adult (G-L). Blue- muscle light chain kinase (MLCK); red-propidium iodide (PI). White asterisk- localization of neo-DIPEN in the adventitia (C, D, I, J). White arrow (F, I, J) aberrant neo-DIPEN staining in the medial layer of the aorta in *Adamts5*$^{-/-}$ mice. Ao-aorta; AV-aortic valves; PA-pulmonary artery. Bar in A=200μm applies to B, G, H; bar in C= 50μm, applies to D-F, I-L.

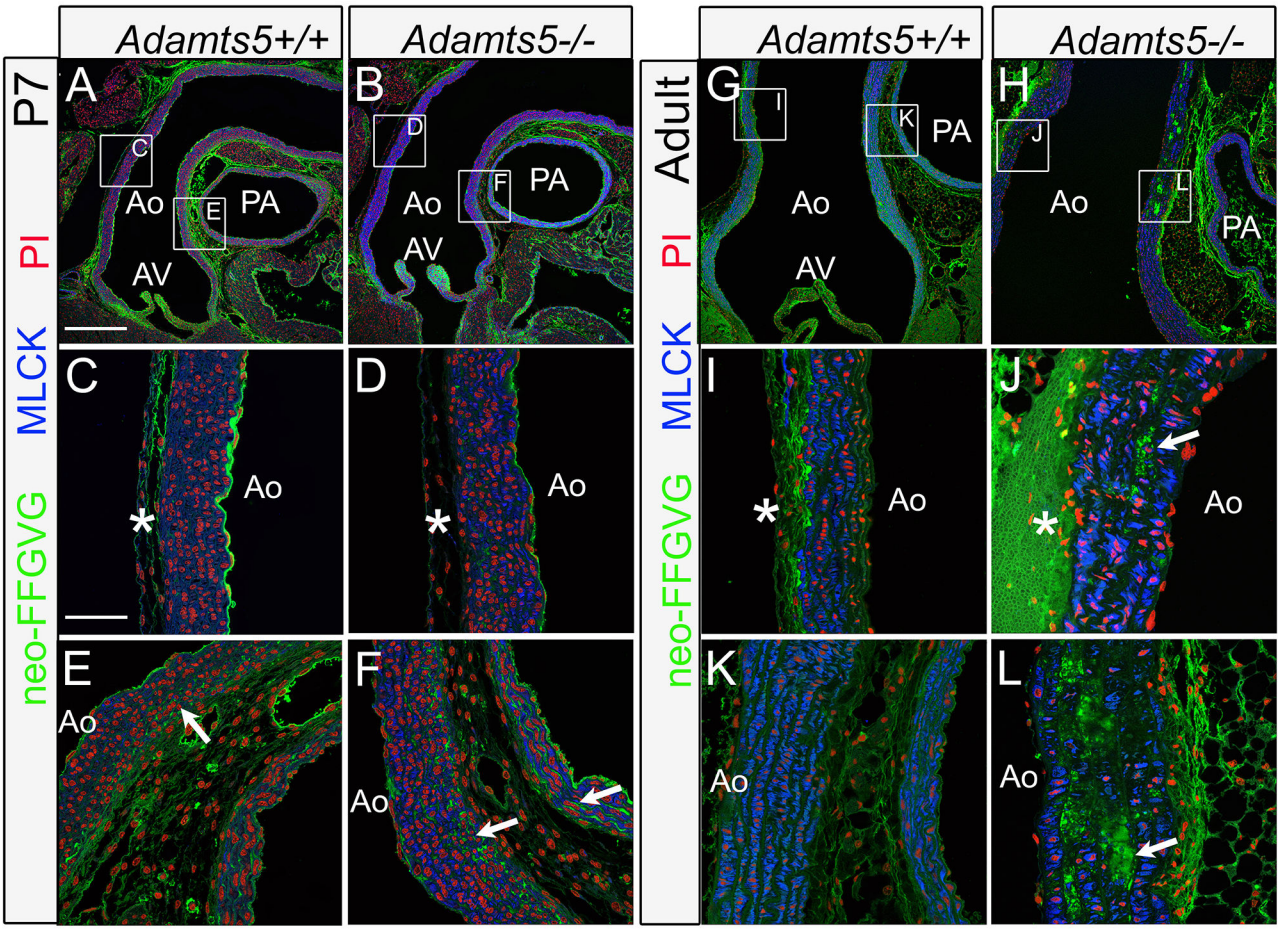

Figure 8: Aggrecan neo-epitope antibody neo-FFGVG correlates with smooth muscle cell loss and exhibits a differential pattern of expression in the ascending aorta of *Adamts5*$^{-/-}$ mice.

Histological sections of *Adamts5*$^{+/+}$ (A, C, E, G, I, K), and *Adamts5*$^{-/-}$ (B, D, F, H, J, L). Boxes in A, magnified in C, E; boxes in B, magnified in D, F; boxes in G, magnified in I, K; boxes in H, magnified in J, L. Immunolocalization of Acan neo-FFGVG (A-L, green), at postnatal day 7 (P7, A-F) and adult (G-L). Blue- muscle light chain kinase (MLCK); red- propidium iodide (PI). White asterisk- neo-FFGVG in the adventitia (C, D, I, J). White arrow (E, F, J, L) immunolocalization in the medial layer of the aorta. Ao-aorta; AV-aortic valves; PA-pulmonary artery. Bar in A=200μm applies to B, G, H; bar in C= 50μm, applies to D-F, I-L.

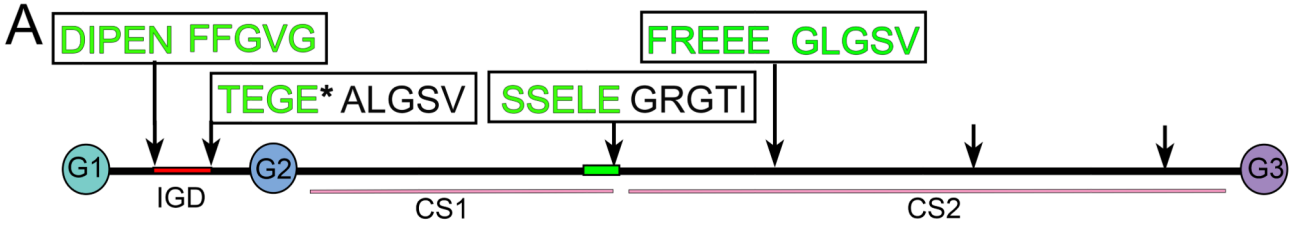

B

Antibody	Age	*Adamts5+/+* Localization		*Adamts5-/-* Localization	
'Intact Acan'	E14	-		++	Medial
	P7	+	Medial	+++	Medial
	1mo	+	Medial	+++	**Int/Medial**
	Ad	+	Medial	+++	**Int/Medial**
FREEE	P7	+/-	Medial	+++	Medial
GLGSV	P7	+/-	Medial	+++	Medial
SSELE	P7	+/-	Medial	+++	Medial
ITEGE*	P7	+++	Medial	+/-	Medial
DIPEN	P7	++	Int/Aventitia	-	Int/Adventitia
	Ad	++	Adventitia	+++	**Medial**
FFGVG -	P7	++	Adventitia	++	**Medial**
	Ad	++	Adventitia	++	**Medial SMC loss**

Figure 9: Summary of differential staining of aggrecan intact and neo-epitope antibodies in the developing and adult ascending aorta of *Adamts5*$^{-/-}$ and *Adamts5*$^{+/+}$ mice.

Schematic of Acan core protein (A) with neo-epitope antibodies utilized (green font). Circles denote globular Acan domains, pink bars depict the glycosaminoglycan binding domains, chondroitin sulfate 1 (CS1) and chondroitin sulfate 2 (CS2). Acan antibodies utilized (B) depicted with a schematic showing the expected fragments. 'Intact Acan' antibody refers to the region of the epitope utilized for the antibody to Acan presented in Fig. 2. E14.5 (embryonic day 14.5), P7-postnatal day 7, Ad-adult (2mo and older). Medial-aortic medial layer expression; Int-aortic intimal layer expression; SMC-smooth muscle cell. Red font in *Adamts5*$^{-/-}$ expression column denotes increased expression in *Adamts5*$^{-/-}$ compared to *Adamts5*$^{+/+}$; blue font denotes decreased expression in *Adamts5*$^{-/-}$. In far right *Adamts5*$^{-/-}$ localization column, bold black font denotes increased expression within the same region as wild type, *Adamts5*$^{+/+}$. Bold red font in the far-right *Adamts5*$^{-/-}$ column,

indicates change in localization and increased immunoreactivity of antibodies in *Adamts5*$^{-/-}$ hearts.